ELSEVIER

Contents lists available at ScienceDirect

Materials and Design

journal homepage: www.elsevier.com/locate/matdes



Near-fiber effects of UV irradiation on the fiber-matrix interphase: A combined experimental and numerical investigation



Libin K. Babu^a, Kunal Mishra^a, Raman P. Singh^{a,b,*}

^aSchool of Mechanical and Aerospace Engineering, Oklahoma State University, Stillwater, OK 74078, USA

HIGHLIGHTS

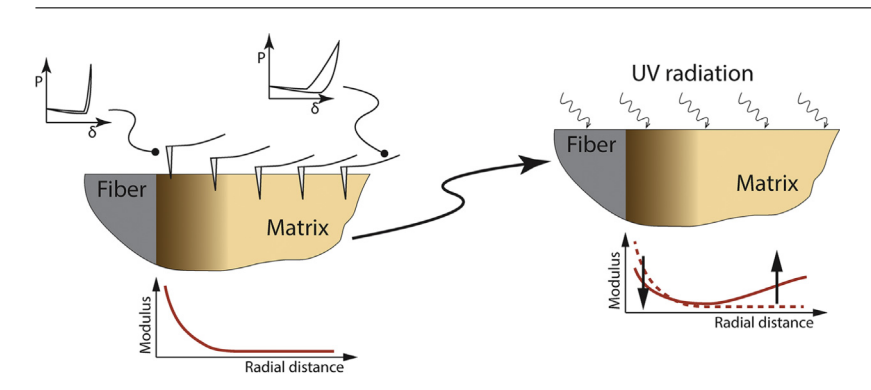
- An apparent increase in interphase modulus due to fiber constraint is limited to 40 nm away from fiber.
- The contribution of fiber constraint is less significant considering gradient in interphase modulus.
- Response of epoxy to UV irradiation is influenced by the proximity to the fiber reinforcement.
- Photocatalytic degradation of carbon fiber due to UV irradiation impacts interphase modulus.

ARTICLE INFO

Article history: Received 11 May 2018 Received in revised form 21 July 2018 Accepted 23 July 2018 Available online 26 July 2018

Keywords: Carbon fiber composites Interphase Fiber-constraint UV irradiation AFM indentation

GRAPHICAL ABSTRACT



ABSTRACT

Characterization of the interphase region in carbon fiber reinforced polymer (CFRP) is challenging because of the length scale involved. The interpretation of measured load-displacement curves using indentation is affected by the lack of analytical solutions that account for the fiber constraint effect. A combination of AFM (Atomic Force Microscopy) based indentation and FE (Finite Element) simulations showed a gradient in the elastic modulus of the interphase evaluated along a radial line from the fiber. 3D FEA (Finite Element Analysis) indicated that fiber constraint effect is significant in the region less than 40 nm away from the fiber. Nonetheless, the apparent rise in elastic modulus due to fiber constraint is limited when compared to the gradient in the elastic modulus of the interphase. Additionally, this technique is used to demonstrate that UV irradiation causes a rapid decrease in the modulus of the region near the fiber due to photocatalytic degradation of carbon fiber but subsequently increases due to high cross-linking. Whereas, the modulus of the matrix at 8 mm away from the fiber decreased by 32% after 24 h of UV irradiation. This indicates that the response of epoxy to UV irradiation is influenced by the proximity to the reinforcement.

© 2018 Elsevier Ltd. All rights reserved.

1. Introduction

Fiber-reinforced polymer-matrix composites find extensive application across various sectors including transportation, energy

generation, aerospace, and infrastructure. This can be attributed to the exceptional properties of composite materials such as high strength to weight ratio and high modulus [1,2]. Furthermore, the design and fabrication process can be tailored to generate direction-dependent material properties [3]. Nonetheless, understanding and predicting the influence of near-fiber region on the long-term durability of composite materials and its performance under harsh environments continue to be a matter of concern [4,5]. Characterizing

^bSchool of Material Science and Engineering, Oklahoma State University, Tulsa, OK 74106, USA

^{*} Corresponding author. E-mail address: raman.singh@okstate.edu (R.P. Singh).

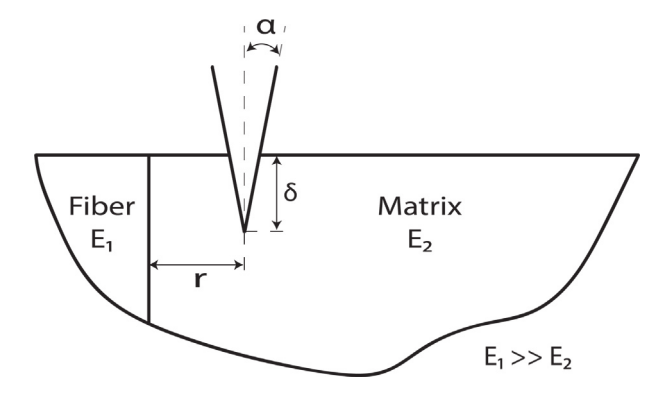


Fig. 1. Schematic of indentation in interphase region.

the mechanical response, damage tolerance, and long-term durability of these materials is further complicated because it involves the response of the two individual components, namely the fiber and the matrix, and also by the interaction between the two. This study is focused on the near-fiber region known as interphase, which is often characterized by a matrix material with properties distinct from the rest of the bulk material [6]. Its presence is a result of the chemical interaction between the fiber and the matrix, during the curing process in composites [7]. The response of the interphase region governs the load-transfer mechanisms in composites and can be considered as an important determinant of the type of failure and the overall load bearing capabilities of the composite material [4]. The following sections discuss the challenges associated with the determination of true properties of the interphase region at very small length scales and the impact of severe environmental conditions such as UV irradiation on the nano-scale properties.

1.1. Span of fiber-matrix interphase and influence of fiber constraint

The interphase properties as well as its width are dependent on the materials considered and can be influenced by fiber surface treatments [8-10]. The width of the interphase region in polymermatrix composites has been found to vary from several hundred nanometers to few micrometers, depending on the chemical interaction between fiber and matrix [11,12]. Due to the small length scale of the interphase region, several nanomechanical methods based on tip–specimen interaction have been developed to characterize the interphase region. These include instrumented nanoindentation [13,14], nano-scratch techniques [15], and atomic force microscope

(AFM) indentation [16-18]. Nonetheless, the application of the above described methods to determine the mechanical properties of the interphase region is limited by the assumption of an unconstrained space, as all of the solutions available are for indentation in a semi-infinite half-space [19]. In the case of indentation in the interphase region, the loading is applied in the vicinity of a rigid boundary (note that the elastic modulus of fiber is very large as compared to the matrix), as indicated in Fig. 1. This produces a constraint effect or a fiber-bias in the indentation data, which requires the use of appropriate solutions to determine material properties from the load versus displacement data. However, most indentation studies on the behavior of interphase region completely ignore or only partially address the influence of the fiber constraint.

Stresses produced in the material during indentation, interact with the rigid boundary condition produced by the vicinity of the fiber. This leads to the overestimation of the mechanical properties in the region. Kumar et al. [20] described this as a phenomena due to "the slowing down in the uniform flow of the bulk material", just below the indent near the stiffer fiber. Pascual et al. [13] pointed out that the interaction of the stress field beneath the indenter and the nearby fiber can lead to a wrong estimation of the width of interphase. Li et al. [21] described that there is a 'mutation' of the load-displacement curve due to a fiber stiffening effect. It was noted that the effect of variation in modulus of matrix is negligible, but this variation was very sensitive to changes in indentation depth. Hu et al. [22,23] discussed an apparent gradient in the modulus of the fibermatrix interphase region due to fiber constraint. They also observed that fiber bias is directly proportional to the depth of indentation. The lack of a good contact theory for indentation of anisotropic and non-homogeneous materials was acknowledged. Young et al. [16] presented the measure of torsion on AFM cantilever as a method to identify influence of local reinforcement in determination of the size of the interphase.

While these studies consider the effect of constraint on the indentation results, they do not provide an explicit scheme for quantifying this effect or for decoupling the fiber-bias effect from the actual variation in interphase properties. Studies by Hardiman et al. [24,25] suggested the concept of a 'fiber constraint factor' (FCF) to evaluate suitable indentation depths at which fiber bias can be ignored. The FCF considered in their work, is influenced by the circularity of the matrix pockets. Nonetheless, their work is limited to a Berkovich indenter, which has a much greater effective cone angle as compared to a AFM tip. Belec and Joliff [17] noted the impact of actual probe geometry on the mechanically affected zone in AFM force measurements. Brune et al. [26] conducted direct measurements of the stiffness of rubber interphase and indicated the possible

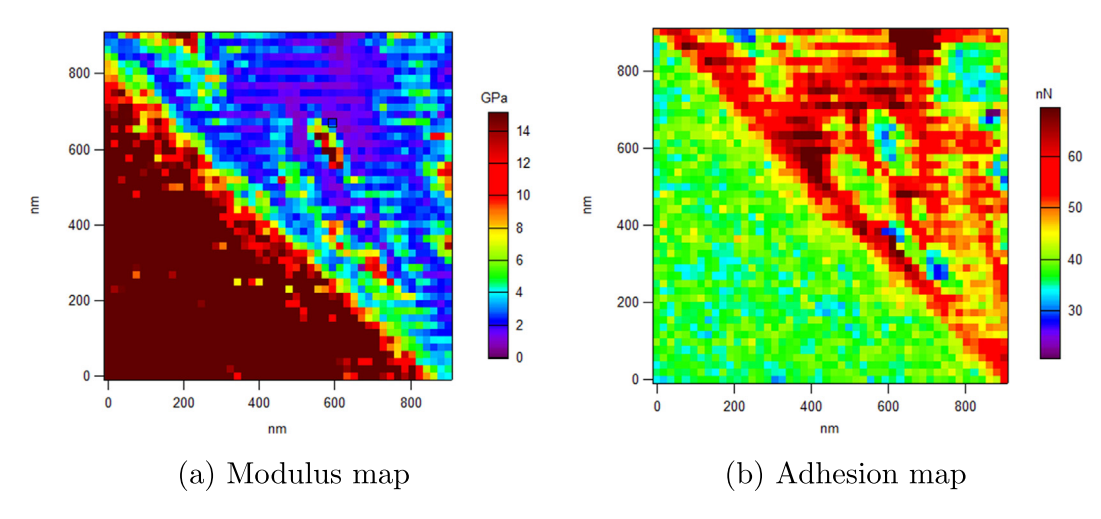


Fig. 2. AFM plots of interphase region in carbon fiber reinforced epoxy.

impact of 'probe effect along with wall effect' on the interphase measurements. A recent review by Roy et al. [27] on the characterization of polymer nanocomposites noted the challenge in eliminating artifacts from the interphase measurements and also remarked that AFM measurements along with Finite Element (FE) modeling will be able to overcome these challenges. Very recently, adaptive optimization technique using numerical modeling is presented as a possible method to study the interphase properties in polymer nanocomposites by Wang et al. [28].

In this study, the first objective is to employ AFM-based indentation combined with 3D Finite Element Analysis (FEA) to ascertain the radial distance from the fiber where the impact of fiber constraint is seen on the measurements of the interphase properties.

1.2. Effect of UV irradiation in near-fiber region

Exposure of polymers to UV radiation leads to the absorption of photons and the activation of polymer macromolecules causes breaking of bonds and the formation of free radicals: which over extended periods of exposure will lead to the failure of the polymer [29]. Chemical structure of the polymer is changed by chain scission which leads to the formation of functional groups with double bonds such as C=C and C= O. These functional groups involved in the degradation process leads to the discoloration of the polymer [30]. Woo et al. [29] observed brittle fracture of epoxy due to UV embrittlement with limited amount of plastic deformation. It was noted that rate of degradation is very rapid initially and shows slight increase with further exposure. Mailhot et al. [31] indicated that changes in the properties of these polymers are dependent on the amount of chain scission that occurs during its exposure to UV. They investigated the photooxidation mechanism of diglycidyl ether of bisphenol-A (DGEBA) and amine based hardener. The major chemical changes upon exposure to UV involved the disappearance of ether group (CH_2) and the breaking of the CH_3 —C bond. As it is largely governed by chain scission reactions the properties of the polymer can decrease after exposure to UV.

In addition, past research have provided information about the photocatalytic degradation of graphene which is quite identical to carbon fiber in terms of chemical structure. Mulyana et al. [32] observed that graphene subjected to UV/O3 treatment followed by UV irradiation underwent oxidation and subsequent reduction reactions, that led to the generation of free radicals. These free radicals can influence the chemical response of polymers in fiber reinforced composites to UV irradiation. Awaja and Pigram [33] indicated that the type of reinforcement influences the response of matrix such as epoxy due to degradation by UV exposure. They observed that carbon fiber reinforced epoxy underwent chain scission and cross-linking (formation of new covalent bonds between the chains or recombination of radicals) reactions during UV irradiation. X-ray photoelectron spectroscopy (XPS) of UV exposed CFRP revealed an increase of 108% in carbonyl species (C= 0), which indicated the impact of surface oxidation. It was noted that the increase in reaction sites resulting from chain scission leads to more opportunities for oxygen and nitrogen to form bonds with polymer, thereby causing a rise in cross-linking reactions.

Therefore it is evident that exposure to UV rays can lead to substantial degradation of the fiber, bulk material and interphase. Recently, Niu et al. [34] observed that the width of the interphase in carbon fiber reinforced poly(ether-ether-ketone) composite decreased due to ultraviolet and hydro-thermal exposure. In the subsequent work by Niu et al. [35], it is shown that the modulus value of matrix in carbon fiber reinforced poly(ether-ether-ketone) composite showed an initial increase due to UV irradiation and condensation on account of the chemical cross-linking. However, there has been very limited focus on studying the influence of reinforcement on variation of interphase properties as a function of time

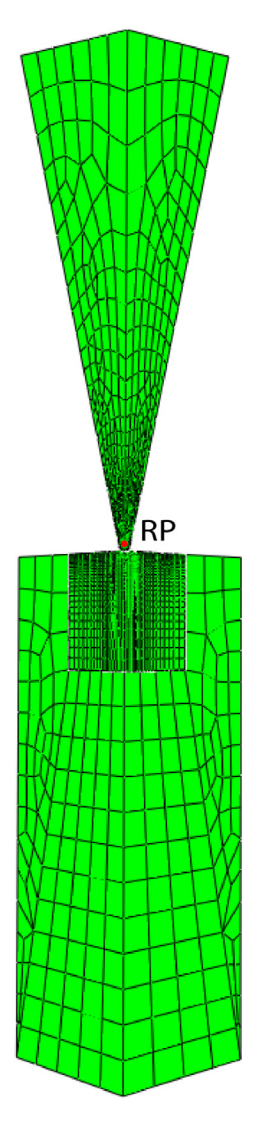


Fig. 3. 3D model representing AFM indentation.

exposed to UV radiation and radial distance to the fiber. Hence, the second objective of this work is to explore the impact of UV irradiation on the properties of the interphase and matrix as a function of both time of exposure and distance from the carbon-fiber reinforcement.

2. Materials and methodology

2.1. Generation of elastic modulus maps using AFM indentation

In this study, interphase samples were prepared by embedding carbon fibers in an epoxy matrix. Carbon fiber tows with 6k filament count were obtained from Hexcel (Stamford, CT, USA). These fibers have a proprietary surface treatment done by the manufacturer. The polymer matrix was prepared using a diglycidyl ether of bisphenol- F (DGEBF) based epoxy resin (EPON $862^{\$}$), cured using an aliphatic amine based hardener (EPIKURE $3274^{\$}$). Both epoxy and hardener were acquired from the Miller-Stephenson Chemical Company (Dunbury, Connecticut, USA). Curing was done at room temperature for 24 h and post-curing at 121 °C for 6 h. Small circular blocks of samples were cut using precision cutter (ISOMET 1000, Buheler, Lake Bluff, Illinois, USA) and polished using metallographic techniques starting from 320 grit grinding paper to 0.05 μ m alumina particles

using an automated polisher (Labopol 5, Struers, Cleveland, Ohio, USA). Initially sample preparation was done by cryo-microtoming using a diamond knife. But it was observed that cryo-microtoming led to distortion of the fiber and also epoxy smeared over the carbon fiber; making it difficult to obtain clear images of the surface. Therefore cryo-microtoming was omitted from subsequent material preparations.

An atomic force microscope (MFP–3D, Asylum Research, Santa Barbara, CA, USA) was used for imaging and force spectroscopy of the prepared samples. The AC160TS AFM tip, manufactured by Olympus Micro Probes (Center Valley, PA, USA), which is recommended for study of polymers, was employed. The cantilever has a resonant frequency in air of $300 \, \text{kHz} (100-200 \, \text{kHz})$ and a typical spring constant of $26 \, \text{N/m} (8.4 \, \text{to} \, 57 \, \text{N/m})$. Images of the carbon fiber and epoxy interphase were collected in tapping mode. A dip in the height profile of top of the fiber was observed; it can be regarded as a surface artifact due to mechanical polishing of the sample. The root mean square roughness (R_q) of the surface after polishing was found to be approximately 4 nm. The indentation depths for force spectroscopy have to be substantially greater than the surface roughness, in order to minimize the influence of surface artifacts on the data collected.

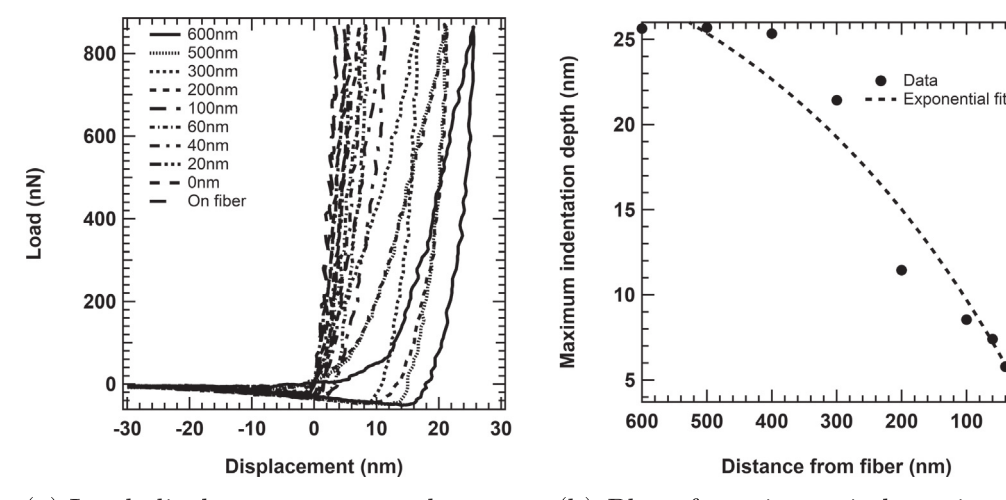
Prior to force spectroscopy, calibration of the AFM cantilever was done to determine the spring constant and inverse optical lever sensitivity (InvOLS). Sader method [36], which was incorporated in the software was utilized to estimate the two parameters. The spring constant and InvOLS were observed to be about 42 N/m and 56 nm/V, respectively. Force spectroscopy of the carbon fiber and epoxy interphase was done in contact mode using force as the trigger channel. Force maps were generated at different points across the interphase using a 48 \times 48 grid placed over 950 \times 950 nm. The load controlled indentations were conducted with a maximum load of 870 nN. The maximum observed indentation depth was 27 nm. Fig. 2a shows the modulus map generated by 'full field' force displacement curves. Every point on the modulus map uniquely represents the elastic modulus obtained from each of the 2304 load-displacement curves. The modulus values were generated using the in-built tool based on Oliver-Pharr method [19]. It was difficult to precisely distinguish the contour of the carbon fiber using the modulus map. Therefore adhesion map shown in Fig. 2b was used to estimate the contour of carbon fiber. It can be observed that the adhesion of the tip is higher on the epoxy than the carbon fiber; making it possible to determine the position of the fiber boundary in the image with ease.

It can be observed using the color scheme that the modulus of carbon fiber is shown as 15 GPa, which is significantly lower than its nominal value. This can be attributed to the limitation of the AFM tip used. The load–displacement curves obtained in the interphase region will be used to validate the simulation of AFM indentation.

The modulus maps generated using AFM based force spectroscopy included 2304 load–displacement curves spread across the fiber, interphase and matrix. In order to obtain meaningful interpretation of the collected data, a MATLAB code was written. Key objective of this step was to capture data along radial lines from the boundary of the fiber. As described previously, adhesion map was used to identify the points on modulus map corresponding to the boundary of the fiber and it was given as input to the MATLAB code. Using basic mathematical equations of circle, a portion of circle was superposed over the boundary of the fiber and the center of the circle was also determined. Equation of radial line was then employed to form radial lines from the boundary of the fiber. Points along each radial line were obtained as the output of the code.

2.2. Finite element modeling of AFM indentation

The distinct properties of interphase region is due to variation in material properties of the region and influence of fiber constraint. Commercial finite-element software ABAOUS v2016 (Dassault Systèmes, Vlizy-Villacoublay, France) was used to model and simulate AFM indentation in 3D space. The variation in materials properties of the interphase were not taken into account in simulations of AFM indentation and therefore it was possible to determine the impact of fiber bias alone on the measured properties. 3D finite element modeling of AFM indentation required the creation of a model representing the AFM indenter. Scanning electron microscope (SEM) images of AFM tip, AC160TS, obtained from Asylum Research, Santa Barbara, CA, USA, were used to develop the model representing the tip. Considering a maximum indentation depth of 27 nm observed in experiments, geometric dimensions of the indenter up to a height of 800 nm from the apex were collected. The front angle of the tip is 0°~and back angle is 35°. The tip was observed to be rounded with a radius of about 10 nm. The indenter was modeled as discrete rigid as its elastic modulus is very high as compared to the specimen and its degrees of freedom was constrained in the directions perpendicular to the loading. To reduce computational cost and to provide finer mesh at the point of indentation, specimen



(a) Load–displacement curves along a ra- (b) Plot of maximum indentation depth dial line from the fiber with distance to the fiber

Fig. 4. AFM indentation data.

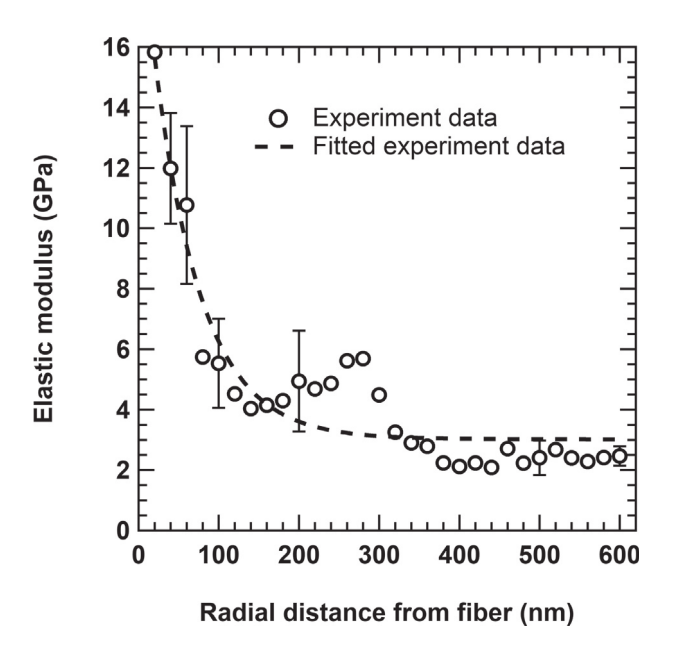


Fig. 5. Average variation of the elastic modulus evaluated from experiment along with exponential fitted curve as function of distance from fiber.

was modeled as two parts using 8 node brick element with reduced integration elements (C3D8R) with minimum element size of 1 nm. The first part was modeled as a deformable wedge shaped insert of 60° and 50 nm length with extra fine mesh, as large local deformation takes place in this region. The other part was a supporting wedge shaped structure of coarse mesh with all the dimensions set as 300 times the maximum observed indentation depth, to ensure far field effects were negligible. A tie constraint was used to connect the two parts. Fig. 3 shows the 3D FE model representing the AFM indentation. As the AFM manufacturer, Asylum Research (Santa Barbara, CA, USA) had indicated that the AFM tip indents at an angle of 10° with the specimen, the indenter tip was placed at 10° with the top surface of the specimen.

Displacement controlled indentations were done in 3D space to minimize instabilities in the simulations. Frictionless contact was assumed between the indenter and the specimen. Experimental data was used to specify the elastic properties of the specimen as elastic modulus, E = 2.78 GPa and Poisson's ratio, $\nu=0.34$. Plasticity was defined using yield strength determined as 92.7 MPa by compression tests carried out on epoxy samples. Isotropic hardening was used to model the hardening behavior of the specimen. Ramberg–Osgood model given in Eq. (1) was fitted to the compression test data to evaluate the yield offset, $\alpha(\frac{\sigma_0}{E})$ and hardening exponent, n. Where, σ_0 refers to the yield stress and E denotes elastic modulus. Multiplier and exponent were evaluated as 0.0593 and 0.99, respectively.

$$\epsilon = \frac{\sigma}{E} + \alpha \frac{\sigma}{E} \left(\frac{\sigma}{\sigma_0}\right)^{n-1} \tag{1}$$

A 4-node 3-D bilinear rigid quadrilateral element (R3D4) was used to mesh the indenter. Encastre boundary condition was specified to right-hand end of the specimen to represent the rigid fiber constraint. A roller boundary condition was applied to the bottom region of the specimen. Additionally, the degree of freedom perpendicular to the sides of the specimen were constrained to remove instabilities. Surface to surface interaction was defined between the indenter (master) and the top surface of the specimen (slave). Loading and unloading for the simulation were defined as independent static general steps. The NLGEOM option was used to account for the nonlinearities present in the deformation. The reaction force (RF) at

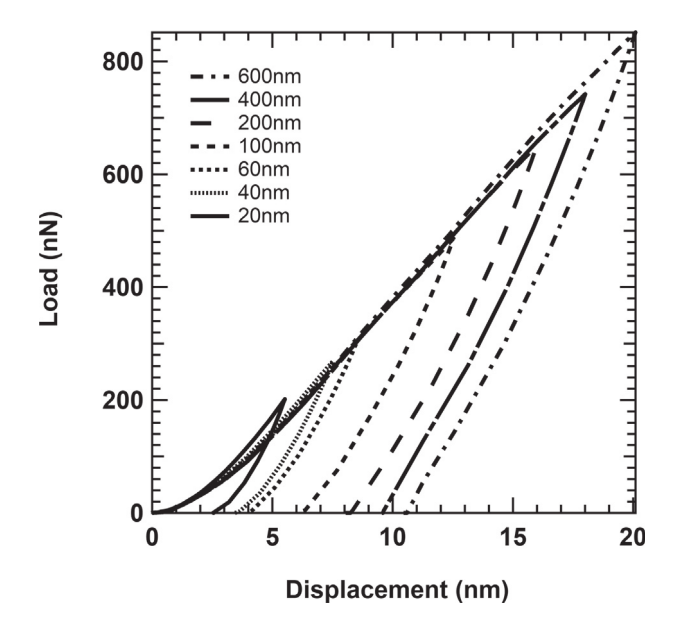


Fig. 6. Load-displacement curves obtained using 3D FEA model of AFM indentation.

the reference point (RP) of the indenter, along the axis of loading was collected as the load data. The displacement in the direction of loading of the left top corner node of the wedge shaped specimen i.e. just beneath the indenter tip was recorded as the displacement data.

Simulations were done at different distances from fiber, denoted by r in Fig. 1 to determine the impact of fiber constraint on the measured properties of the near fiber region. The values of r were selected keeping in view of the resolution of modulus map obtained experimentally and included values: $600 \, \text{nm}$, $400 \, \text{nm}$, $200 \, \text{nm}$, $100 \, \text{nm}$, $60 \, \text{nm}$, $40 \, \text{nm}$ and $20 \, \text{nm}$. Average of indentation depths at the different value of r observed in experiments were used for the simulations.

2.3. Determination of impact of UV irradiation

As discussed previously, Awaja and Pigram [33] had noted that the response of epoxy to UV irradiation can be dependent on the type of reinforcement. Therefore AFM force spectroscopy was used to investigate the impact of UV irradiation on the near fiber region and matrix away from the vicinity of the fiber. The purpose of studying the variation in properties of epoxy significantly away from the fiber was to create a reference value for the analysis of variation in properties of interphase region as a function of time exposed to UV irradiation and distance of the indent from the fiber. Carbon fiber reinforced epoxy samples were exposed to ultraviolet radiation (UV) for time periods varying from 30 min to 24 h, using QUV accelerated weathering tester (Q-labs, Westlake, OH, USA). Thereafter, AFM based force spectroscopy was used to study the properties of these samples.

3. Results and discussion

3.1. Experimental data analysis

Fig. 4 (a) shows the variations in load–displacement curves along one such radial line from the fiber. It can be noted that there is a 'shift' in the load–displacement curves as the indentations were done closer to the fiber. Fig. 4 (b) provides a similar observation which shows that for the same maximum indentation load, the maximum indentation depth was reduced significantly while indenting closer to the fiber. The ripples in the load–displacement data can

be attributed to the noise from feedback loop and other electrical signals of the equipment. Fast Fourier Transform was used on the load-displacement curves to determine the frequency of the data and a low pass filter (LPF) was then used to remove the noise and extract the true data. In Fig. 4 (a), the portion of the curve beyond unloading region indicated adhesion between the tip and the sample. It can be noted that there was significant adhesion away from the fiber i.e.~for indents on the matrix, compared to the fiber.

Elastic modulus of the carbon fiber reinforced epoxy was also studied along the radial line from the fiber. Fig. 5 shows the average elastic modulus values along 20 radial lines that were plotted as a function of the distance from fiber. As resolution of the modulus map was 20 nm, data analyzed along the radial line was extracted for each increment of 20 nm. It can be observed from Fig. 5 that there exists a gradient in the modulus values along the radial line. An exponential curve given by the dashed line in Fig. 5, was used to fit the change in modulus values along the radial lines from the boundary of the fiber. Based on the change in elastic modulus values, the width of the interphase region was determined to be approximately 250 nm. As noted previously, the increase in elastic modulus of the interphase determined by indentation technique can be a combination of the variation in material properties of the region and the influence of fiber constraint.

It can be observed from Fig. 5 that the error bars for average modulus values away from the fiber are very small compared to those near the fiber. This can be attributed to the fact that the indentation depths are much higher for force mapping done in region away from the fiber than the indents carried out closer to the fiber. In addition, the influence of surface roughness becomes more evident at shallow indentation depths, leading to significant variability. But as shown in Fig. 5, the existence of variation in modulus along the radial line can be confirmed, taking into confidence the span of error bars. However as discussed previously, it is important to distinguish the apparent rise in modulus due to fiber bias because accurate determination of interphase properties will provide precise assessment of performance of the composite structure.

3.2. Analysis of simulation data

Fig. 6 shows the the load-displacement curves obtained from 3D FEA models of AFM indentation. It can be observed that for the

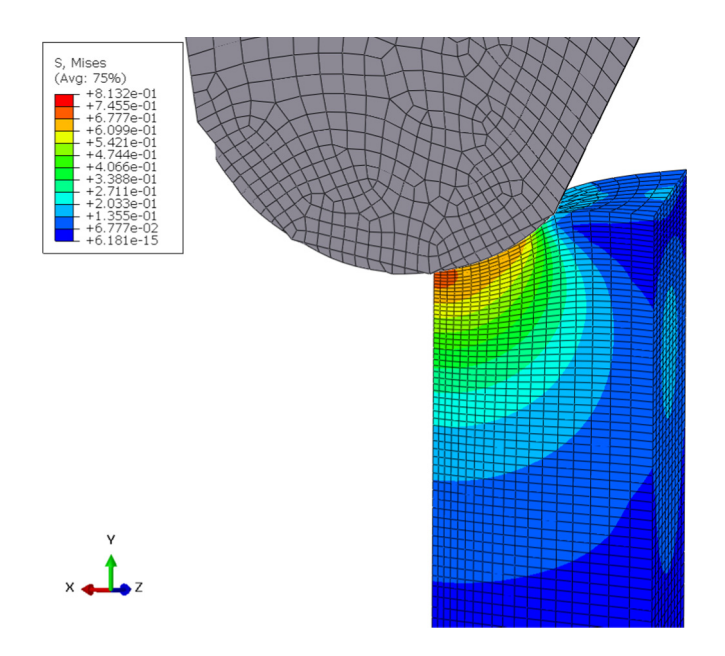


Fig. 7. Interaction of stress field with fiber while indenting close to the representative rigid constraint.

indents done on the same material, there is a shift in the load-displacement curves for indents at 20 nm and 40 nm away from the fiber. This can be attributed to the stiffer response due to the interaction of indentation generated stress contours with encastre boundary representing the rigid fiber, as shown in Fig. 7. The AFM indenter's shape and indentation depth are factors affecting the impact of fiber constraint on the evaluation of properties of near-fiber region. Oliver–Pharr method [19] was used to evaluate the elastic modulus from the load–displacement curves at different distances from the fiber. The elastic modulus of the polymeric matrix – epoxy was determined from indentation at 600 nm away from the fiber as 2.76 GPa.

Fig. 8 shows the comparison of elastic modulus evaluated from experiment with the values obtained from 3D FE simulations. The dashed curve and solid curve represent the exponential fitted curves for experimental and simulation data, respectively. Similar to the observation in Fig. 6, it can be noted that the impact of fiber constraint is considerable only in region less than 40 nm away from the fiber. In the case of 3D model, there is an apparent increase in elastic modulus due to fiber constraint by 108% and 20% at 20 and 40 nm away from the fiber, respectively. It shows for the first time quantitatively that AFM indentation is not as affected by the fiber-bias as Berkovich indentation. This is due to the reason that the effective cone half-angle of the AFM indenter is very small compared to the Berkovich indenter.

It can be observed in Fig. 8 that the increase in elastic modulus values due to fiber constraint is not very significant when compared to the experimentally determined overall gradient in elastic modulus, taking into confidence the error bars. Therefore, it can be confirmed that the mechanical properties of interphase region is distinct from bulk material, while taking the fiber constraint into consideration.

3.3. Variation in elastic modulus due to UV irradiation

The elastic modulus maps across a square region of $5 \mu m$ of epoxy approximately 8 mm away from the carbon fiber in the pristine condition and subjected to 24 h UV irradiation condition are given in Fig. 9 (a) and (b), respectively. Modulus maps for each sample were created using a 48 \times 48 square grid, which implies there were 2304

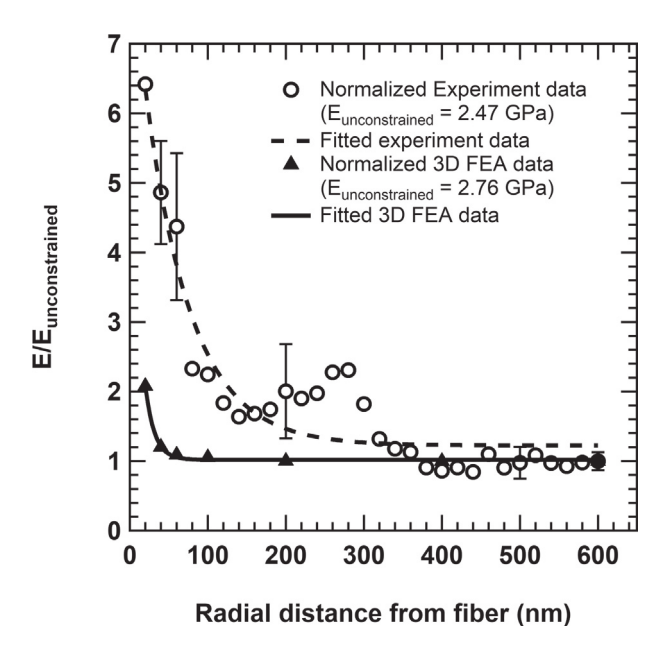


Fig. 8. Comparison of elastic modulus evaluated from experiment and 3D FEA data.

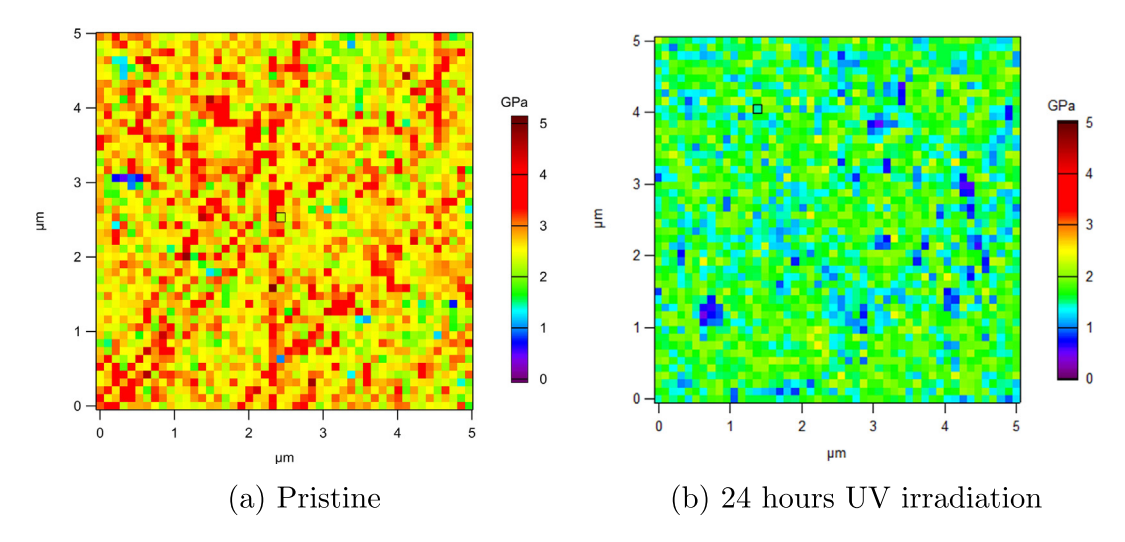


Fig. 9. Modulus maps of epoxy.

load–displacement curves. It can be visually ascertained from the modulus maps that the elastic modulus of epoxy away from the fiber has decreased as a function of prolonged exposure to UV radiation. This is consistent with previously cited literature that shows formation of free radicals as epoxy undergoes chain scissions due to UV irradiation, making it comparatively less stiff. The elastic modulus of pristine epoxy decreased almost linearly from 2.78 GPa to 1.89 GPa after 24 h of UV irradiation. These reported modulus values are the average from all the indents shown in the modulus map.

To study the impact of UV irradiation in near fiber region, elastic modulus maps across 950 nm square region containing the fiber and the interphase were obtained for pristine condition and 6 h of UV irradiation condition, as shown in Fig. 10 (a) and (b), respectively. It can be observed that is severe distortion in fiber contour as well as significant changes in the properties of the near fiber region due to UV irradiation.

The MATLAB code that was previously described was employed to analyze the modulus values of CFRP along radial lines from the fiber. Fig. 11 compares the average modulus values at different radial distances from the fiber in CFRP to the modulus value of epoxy significantly far away from the vicinity of the fiber, as a function of time exposed to UV radiation. Due to the difficulty to ascertain the contour of the carbon fiber because of severe distortion of the carbon fiber, the modulus map of interphase region after 24h of UV

irradiation was not included in the data analysis using the MATLAB code. It can be noted from Fig. 11 that the modulus values at 20 nm and 40 nm away from the fiber decreases rapidly when it is initially exposed to UV radiation, compared to the decrease in modulus values at 100 nm and 600 nm. This can be attributed to the significant amount of chain scission that occurs around the fiber due to the photocatalytic degradation of carbon fiber. This causes the breaking of C—C bonds that leads to formation of O free radicals and new reaction sites near the fiber. After 1 h of UV irradiation, it can be observed that the modulus values at 20 nm, 40 nm, 100 nm and 600 nm rise due to the increase in cross-linking reactions. Hence, after 6 h of UV irradiation the modulus value of epoxy at 600 nm away from the fiber was about 162% higher than the modulus value of epoxy evaluated approximately 8 mm away from the fiber. The modulus of epoxy at about 8 mm away from the fiber decreased monotonically as a function of time exposed to UV radiation due to photo-degradation of epoxy and its response was not influenced by the presence of carbon fiber. Nonetheless, it can be observed that after 6 h of UV irradiation epoxy at 20 nm and 40 nm away from the fiber, showed an overall decrease of 44% and 30%, respectively. It can be attributed to the weakening caused by photocatalytic degradation of carbon fiber. Whereas, the modulus value of epoxy at 100 nm and 600 nm after 6h of UV irradiation indicated an increase of 68% and 124%. respectively. This clearly demonstrates that the presence of carbon

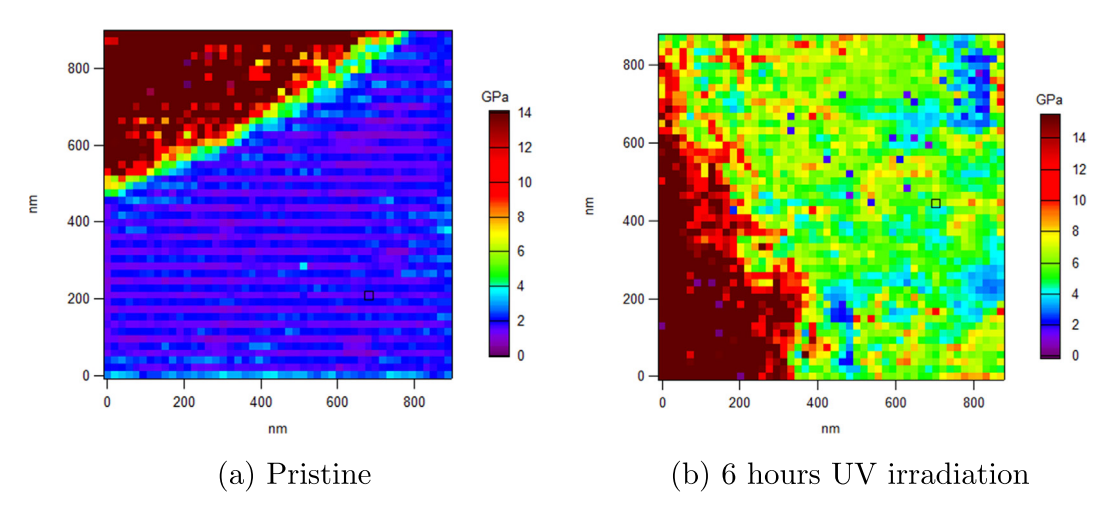


Fig. 10. Modulus maps of carbon fiber reinforced epoxy.

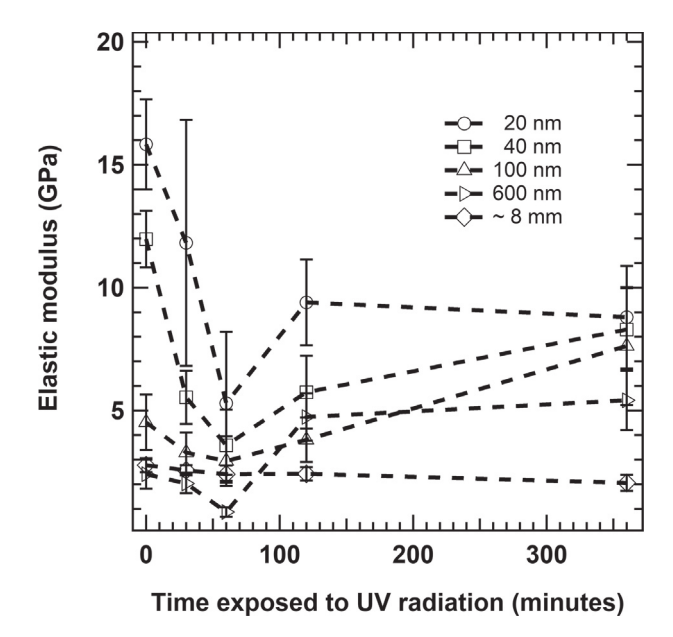


Fig. 11. Variation in the elastic modulus, *E*, of CFRP as a function of time periods of UV exposure for different positions of indent from the fiber.

fiber as reinforcement significantly influences the response of epoxy to UV irradiation.

4. Conclusion

An integrated approach involving AFM-based indentation and FEA modeling is employed to evaluate the extent of influence of fiber constraint on the properties determined in the interphase region. AFM-based force mapping provides high spatial resolution, which is useful in the study of interphases that are small in length scale. The lack of contact theory to directly evaluate mechanical properties using indentation technique, in the presence of a rigid boundary, is resolved by the use of a 3D FEA model of AFM indentations. The width of interphase in carbon fiber reinforced epoxy is determined to be 250 nm, based on the gradient in interphase properties. The 3D FE simulations indicate that fiber constraint impacts interphase modulus only within 40 nm of radial distance from the fiber while using AFM tip. Nonetheless, the apparent increase in interphase modulus is significantly less as compared to the overall gradient in the modulus value of the region, as determined by AFM indentation. Hence, these results confirm that the behavior of interphase is distinct compared to the bulk material.

AFM based indentations are further utilized to evaluate the impact of UV irradiation on the modulus value as a function of exposed time and radial distance from the fiber. This study demonstrates that the response of epoxy to UV irradiation is dictated by the proximity to the carbon fiber reinforcement. Photocatalytic degradation of carbon fiber causes an initial decrease in modulus value of interphase region through chain scission reactions that lead to possible formation of free radicals and new reaction sites. However, it is observed that with further exposure to UV irradiation, the interphase modulus values increase due to enhanced cross-linking reactions. Overall, the presence of carbon fiber hinders the photo-degradation of epoxy, which suggests that carbon fiber reinforcement could improve the durability of the composites. Further studies involving analysis of sub-surface structure of the composite may be beneficial to determine the complete mechanism of damage of carbon fiber reinforced epoxy caused by UV irradiation.

Data availability

The raw/processed data required to reproduce these findings cannot be shared at this time as the data also forms part of an ongoing study.

Acknowledgments

This material is based upon a work supported by the National Science Foundation, USA under grant no. 1649481. The authors would like to acknowledge the feedback provided by Dr. Gajendra Pandey of The Coca-Cola Company, Atlanta, GA on the numerical modeling aspects of this study.

References

- B.E.B. Uribe, E.M.S. Chiromito, A.J.F. Carvalho, R. Arenal, J.R. Tarpani, TEMPO-oxidized cellulose nanofibers as interfacial strengthener in continuous-fiber reinforced polymer composites, Mater. Des. 133 (2017) 340–348.
- [2] D. Kada, A. Koubaa, G. Tabak, S. Migneault, B. Garnier, A. Boudenne, Tensile properties, thermal conductivity, and thermal stability of short carbon fiber reinforced polypropylene composites, Polym. Compos. 39 (S2) (2016) E664–E670.
- [3] P. Xu, Y. Yu, D. Liu, M. He, G. Li, X. Yang, Enhanced interfacial and mechanical properties of high-modulus carbon fiber composites: establishing modulus intermediate layer between fiber and matrix based on tailored-modulus epoxy, Compos. Sci. Technol. 163 (2018) 26–33.
- [4] N. Kotelnikova-Weiler, O. Baverel, N. Ducoulombier, J.F. Caron, Progressive damage of a unidirectional composite with a viscoelastic matrix, observations and modelling, Compos. Struct. 188 (2018) 297–312.
- [5] Y. Niu, Y. Yang, X. Wang, Investigation of the interphase structures and properties of carbon fiber reinforced polymer composites exposed to hydrothermal treatments using peak force quantitative nanomechanics technique, Polym. Compos. 39 (S2) (2018) E791–E796.
- [6] L. Drzal, Composite interphase characterization, SAMPE Journal, Vol 19, 1983, pp. 7–13.
- [7] H. Gajendran, R.B. Hall, A. Masud, K.R. Rajagopal, Chemo-mechanical coupling in curing and material-interphase evolution in multi-constituent materials, Acta Mech. (217) (2018) 1–22.
- [8] W. Xu, F. Wu, Y. Jiao, M. Liu, A general micromechanical framework of effective moduli for the design of nonspherical nano- and micro-particle reinforced composites with interface properties, Mater. Des. 127 (2017) 162–172.
- [9] J. Karger-Kocsis, H. Mahmood, A. Pegoretti, Recent advances in fiber/matrix interphase engineering for polymer composites, Prog. Mater. Sci. 73 (2015) 1–43.
- [10] M.D.R. Batista, L.T. Drzal, Carbon fiber/epoxy matrix composite interphases modified with cellulose nanocrystals, Compos. Sci. Technol. 164 (2018) 274–281
- [11] V. Cech, E. Palesch, J. Lukes, The glass fiber-polymer matrix interface/interphase characterized by nanoscale imaging techniques, Compos. Sci. Technol. 83 (2013) 22–26.
- [12] Y. Gu, M. Li, J. Wang, Z. Zhang, Characterization of the interphase in carbon fiber/polymer composites using a nanoscale dynamic mechanical imaging technique, Carbon 48 (11) (2010) 3229–3235.
- [13] A.M. Diez-Pascual, M.A. Gómez-Fatou, F. Ania, A. Flores, Nanoindentation assessment of the interphase in carbon nanotube-based hierarchical composites, J. Phys. Chem. C 116 (2012) 24193–24200.
- [14] R.F. Gibson, A review of recent research on nanoindentation of polymer composites and their constituents, Compos. Sci. Technol. 105 (2014) 51–65.
- [15] A. Molazemhosseini, H. Tourani, M.R. Naimi-Jamal, A. Khavandi, Nanoindentation and nanoscratching responses of PEEK based hybrid composites reinforced with short carbon fibers and nano-silica, Polym. Test. 32 (3) (2013) 525–534.
- [16] T.J. Young, L.E. Crocker, W.R. Broughton, S.L. Ogin, P.A. Smith, Observations on interphase characterisation in polymer composites by nano-scale indentation using AFM and FEA, Compos. A: Appl. Sci. Manuf. 50 (2013) 39–43.
- [17] L. Belec, Y. Joliff, Mechanically affected zone in AFM force measurements focus on actual probe tip geometry, Mater. Des. 104 (2016) 217–226.
- [18] D. Wang, T.P. Russell, Advances in atomic force microscopy for probing polymer structure and properties, Macromolecules 51 (1) (2018) 3–24.
- [19] W.C. Oliver, G.M. Pharr, An improved technique for determining hardness and elastic modulus using load and displacement sensing indentation experiments, J. Mater. Res. 7 (6) (1992) 1564–1583.
- [20] R. Kumar, W.M. Cross, L. Kjerengtroen, J.J. Kellar, Fiber bias in nanoindentation of polymer matrix composites, Compos. Interfaces 11 (5-6) (2004) 431–440.
- [21] Y. Li, M. Li, Y. Gu, Z. Zhang, P. Guan, Investigation of the nanoscale mechanical properties of carbon fiber/epoxy resin interphase. I. Analysis of fiber-stiffening effect during the nanoindentation process based on numerical simulation, Polym. Compos. 33 (8) (2012) 1387–1394.
- [22] Z. Hu, K.J. Lynne, S.P. Markondapatnaikuni, F. Delfanian, Material elastic-plastic property characterization by nanoindentation testing coupled with computer modeling, Mater. Sci. Eng. A 587 (2013) 268–282.

- [23] Z. Hu, M. Farahikia, F. Delfanian, Fiber bias effect on characterization of carbon fiber-reinforced polymer composites by nanoindentation testing and modeling, J. Compos. Mater. 49 (27) (2015) 3359–3372.
- [24] M. Hardiman, T.J. Vaughan, C.T. McCarthy, Fibrous composite matrix characterisation using nanoindentation: the effect of fibre constraint and the evolution from bulk to in-situ matrix properties, Compos. Part A 68 (2015) 296–303.
- [25] M. Hardiman, T.J. Vaughan, C.T. McCarthy, The effect of fibre constraint in the nanoindentation of fibrous composite microstructures: a finite element investigation, Comput. Mater. Sci. 64 (2012) 162–167.
- [26] P.F. Brune, G.S. Blackman, T. Diehl, J.S. Meth, D. Brill, Y. Tao, J. Thornton, Direct measurement of rubber interphase stiffness, Macromolecules 49 (13) (2016) 4909–4922.
- [27] S. Roy, J. Ryan, S. Webster, D. Nepal, A review of in-situ mechanical characterization of polymer nanocomposites, Appl. Mech. Rev. 69(5) (050802). (2017)
- [28] Y. Wang, Y. Zhang, H. Zhao, X. Li, Y. Huang, L.S. Schadler, W. Chen, L.C. Brinson, Identifying interphase properties in polymer nanocomposites using adaptive optimization, Compos. Sci. Technol. 162 (2018) 146–155.
- [29] R.S.C. Woo, H. Zhu, C.K.Y. Leung, J.K. Kim, Environmental degradation of epoxy-organoclay nanocomposites due to UV exposure: part II residual mechanical properties, Compos. Sci. Technol. 68 (2008) 2149–2155.

- [30] B.G. Kumar, R.P. Singh, T. Nakamura, Degradation of carbon fiber-reinforced epoxy composites by ultraviolet radiation and condensation, J. Compos. Mater. 36 (24) (2002) 2713–2721.
- [31] B. Mailhot, S. Morlat-Thérias, M. Ouahioune, J.L. Gardette, Study of the degradation of an epoxy/amine resin, 1 photo- and thermo-chemical mechanisms, Macromol. Chem. Phys. 206 (2005) 575–584.
- [32] Y. Mulyana, M. Uenuma, Y. Ishikawa, Y. Uraoka, Reversible oxidation of graphene through ultraviolet/ozone treatment and its nonthermal reduction through ultraviolet irradiation, J. Phys. Chem. C 118 (47) (2014) 27372–27381.
- [33] F. Awaja, P.J. Pigram, Surface molecular characterisation of different epoxy resin composites subjected to UV accelerated degradation using XPS and ToF-SIMS, Polym. Degrad. Stab. 94 (2009) 651–658.
- [34] Y.F. Niu, Y. Yang, S. Gao, J.W. Yao, Mechanical mapping of the interphase in carbon fiber reinforced poly(ether-ether-ketone) composites using peak force atomic force microscopy: interphase shrinkage under coupled ultraviolet and hydro-thermal exposure, Polym. Test. 55 (2016) 257–260.
- [35] Y.F. Niu, Y. Yang, T.Y. Li, J.W. Yao, Effects of UV irradiation and condensation on poly(ether-ether-ketone)/carbon fiber composites from nano- to macro-scale, High Perform. Polym. 30 (2) (2018) 230–238.
- [36] J.E. Sader, J.W.M. Chon, P. Mulvaney, Calibration of rectangular atomic force microscope cantilevers, Rev. Sci. Instrum. 70 (10) (1999) 3967–3969.